Cavitation clusters in lipid systems – the generation of a bifurcated streamer and the dual collapse of a bubble cluster

Peter R. Birkin,[a†] Hannah L. Martin[a], Jack J. Youngs[a], Tadd T. Truscott[b], Andrew S. Merritt[b], Ethan J. Elison[b] and Silvana Martini[c]

[a.] Chemistry, University of Southampton, Southampton, UK, S0171BJ.

[b.] Department of Mechanical and Aerospace Engineering, Utah State University, Logan, UT, 84322-4130, USA.

[c.] Department of Nutrition, Dietetics, and Food Science, Utah State University, Logan, UT, 84322-8700, USA.

† author for correspondence, prb2@soton.ac.uk.

Abstract

Several studies have reported the use of high intensity ultrasound (HIU) to induce the crystallization of lipids. The effect that HIU has on lipid crystallization is usually attributed to the generation of cavities but acoustic cavitation has never been fully explored in lipids. The dynamics of a particular cavitation cluster next to a piston like emitter (PLE) in an oil, was investigated in this study. The lipid systems, which are important in food processing, are studied with high-speed camera imaging, laser scattering and acoustic pressure measurements. A sequence of stable clusters were noted. In addition, a bifurcated streamer was detected which exists within a sequence of clusters. This is shown to originate from two clusters on the PLE tip oscillating with a 180° phase shift in time with respect to one another. Finally, the collapse phase of the cluster is shown to involve a rapid (< 10 μs) two stage process. These results show that the dynamics of cluster formation and collapse is driven by HIU power levels and might have implications in lipid sonocrystallization.

Keywords: Lipids, cavitation, crystallisation, bubbles, clusters, dynamics

Introduction

Cavitation in aqueous environments has been extensively investigated (Lauterborn, Kurz, 2010, Young, 1999). However, acoustic cavitation in edible lipids has received relatively little fundamental investigation (Martini, Tejeda-Pichardo, Ye, Padilla, Shen, Doyle, 2012). Edible lipids provide flavour, mouthfeel, and palatability to foods. In many cases, the amount of solidified lipids and their crystalline network properties provide these desired characteristics. In turn, these characteristics can be tailored by changing processing conditions or the solidification method. To this end, the deployment of high intensity ultrasound (HIU) has gained traction as this technique is able to alter the kinetics of crystallisation of materials (Chen, Zhang, Sun, Wang, Xu, 2013, Higaki, Ueno, Sato, 2001, Martini, Tejeda-Pichardo, Ye, Padilla, Shen, Doyle, 2012, Patrick, Blindt, Janssen, 2004, Suzuki, Hartel, Martini, 2010, Ueno, Ristic, Higaki, Sato, 2003, Ye, Martini, 2015, Ye, Wagh, Martini, 2011, Zhong, Allen, Martini, 2014). However, control over and the understanding of the exact mechanisms and processes which occur in these systems remains uncertain. This lack of fundamental knowledge limits the exploitation of this approach within this highly important arena, as large sets of empirical experiments are needed. Such experiments must be repeated for different lipid materials, which is both laborious and ineloquent.

Clearly, the use of a targeted approach, where the dynamics of the relevant process may be predictable, would be highly desirable. If we consider the fundamental mechanisms available, the ability of HIU to generate and alter the bubble population (Birkin, Leighton, Power, Simpson, Vinc, Joseph, 2003) and their dynamics must be a key area for investigation. These bubble processes or cavitation dynamics will undoubtedly have a profound effect on these systems as they do for other chemical (Flint, Suslick, 1991, Price, 1992, Price, Ashokkumar, Grieser, 2003, Price, Lenz, 1993, Suslick, Hammerton, Cline, 1986, Weissler, Cooper, Snyder, 1950) and physical (Birkin, Offin, Joseph, Leighton, 2005, Vyas, Preece, 1976, Whillock, Harvey, 1997) processes. For example, the effects on nucleation and crystal growth phenomena have been proven to be significant(Chow, Blindt, Chivers, Povey, 2005, Chow, Blindt, Kamp, Grocutt, Chivers, 2004, Higaki, Ueno, Sato, 2001, Ueno, Ristic, Higaki, Sato, 2003). Nevertheless, these key mechanistic processes in lipids have still to be fully mapped. Previous work (Birkin, Foley, Truscott, Merritt, Martini, 2017) has shown that the bubble dynamics observed in an oil environment are different from those observed in aqueous systems. The most interesting observation was that a bubble cluster(Hansson, Kedrinskii, Morch, 1982, Hansson, Morch, 1980) with an unusual shape and specific periodicity could be generated in the oil media. This cluster was associated with a collimated streamer of bubbles that travelled away from the cluster at velocities in the order of 1-10 m s^{-1}. In addition local heating and possible outgassing were identified, all implying significant differences in these oil systems compared to that of water.

Hence, it is timely, particularly considering the technological significance of these materials, to characterise and contrast the cavitation fields that are generated in these environments with the eventual aim of understanding the factors present and their influence on the crystallisation of oils This characterisation stage is the topic of the investigation reported here.

Materials and Methods

Experimental set-up: The experimental set up has been described previously (Birkin, Foley, Truscott, Merritt, Martini, 2017). Briefly, liquid oil was placed in a polycarbonate cell (60 mm x 60 mm x 150 mm) and cavitation was generated using a piston like emitter (PLE, Misonix, XL2000, 23 kHz and Misonix, S-3000, 20 kHz) immersed in vegetable oil. A 3.2 mm diameter tip was employed in all cases. The tip of the PLE was not polished as this was found not to be conducive to the formation of stable clusters in these oil systems (Birkin, Foley, Truscott, Merritt, Martini, 2017). Sonication was initiated and applied continuously through the data capture windows employed by recording the signals a few seconds after the PLE was started. This approach avoids any ring-up processes, which, although interesting, are not considered here. The power reported for the systems used was determined from the amplifiers used and the associated unit given (W_{rms} for the XL2000 and W for the S-3000). Temperature changes, both local and through the bulk, and the calorific input to the system have been detailed elsewhere (Birkin, Foley, Truscott, Merritt, Martini, 2017). Acoustic data, laser scattering and imaging were gathered with the PLE running continuously (to avoid ring-up issues). However, to avoid excessive heating these PLE excitation was terminated after ~10-20 s exposure.

Characterization of bubble dynamics: High-speed imaging, acoustic emission, and laser scattering measurements were recorded during sonication. High-speed imaging (using a Photron APX-RS or SAZ camera and Navitar x12 lens or a Phantom V2011 and a Sigma (105 mm) fixed lens with 50 mm extension tubes) of the region below the tip within the oil system was combined with a calibrated hydrophone (Reson TC4013) positioned 15 ± 5 mm to the side of the tip of the probe (itself 15 mm immersed into the oil). For reference the sensitivity is -2.66 x 10^{-5} V Pa^{-1} at ~22.7 kHz in water (from the data sheet provided from the manufacturer), however, this calibration data cannot be assumed to be accurate within the oil system without further information. Hence, the sensitivity is given for reference only. The hydrophone signals are left as voltage time series but are useful in ascertaining the acoustic emissions present within the system. In addition, although the high-speed camera images were used to identify specific clusters and their dynamics, hydrophone measurements allow for the routine identification of the periodicity of the oscillation of the clusters formed during sonication.

A laser scattering approach (Birkin, Foley, Truscott, Merritt, Martini, 2017; Birkin, Offin, Vian, Leighton, 2011; Offin, 2006) was also deployed below the HIU source. This system is used to follow transient bubble expansion in this environment on the µs timescale and is suitable for the monitoring of bubble dynamics below PLE tips. FFT analysis of the acoustic data was performed using a bespoke data analysis program (Microsoft Visual Basic 2010 and National Instruments Measurement Studio). Briefly, the data was captured on an oscilloscope with the appropriate timing signals controlling both acquisition and cameras experiments. This data was then processed as discrete time windows (related to the periodicity of the PLE) and the frequency spectrum was obtained through a Measurement studio function (National Instruments). A digital oscilloscope (Owon, DS7102V DSO) was used to capture the acoustic and scattering data (sample rate 1 MHz). Air saturated sunflower oil (Independent) or soybean oil (Great Value, Arizona), SBO, was used in the experiments (see legends). The clusters were found to be very reproducible across labs and with different sets of equipment (see above). Images, hydrophone voltage-time histories and scattering data are representative of a larger data set.

Results and discussion

Bubble events generated during sonication: In a previous work, we have described the two main elements of the observed bubble dynamics generated through sonication of an oil. These were the formation of a cluster of bubbles close to the sonicator tip and a streamer of bubbles (that are generated by this cluster) that move away from the PLE tip (Birkin, Foley, Truscott, Merritt, Martini, 2017). One of the experimentally observable characteristics of these lipid systems under these conditions is that a set of clear audible 'notes' can be detected by ear. These 'notes' change as the amplitude of the sound source is altered. In brief, as the amplitude of tip oscillation was increased (through using higher settings in the sonicator) the cluster of bubbles that formed at the tip of the PLE were found to oscillate at a reduced frequency with respect to the frequency of the source deployed (Birkin, Foley, Truscott, Merritt, Martini, 2017). These cluster frequencies were found to be stable, over an extended period for many seconds, for particular sonicatorsettings. For these stable clusters, their frequency of oscillation are defined as f/N where f is the frequency of the PLE used and N is an integer value. The audible 'notes' are then attributed to the particular periodicity of the stable cluster that forms under the PLE for any given set of conditions and its associated acoustic emission (Birkin, Foley, Truscott, Merritt, Martini, 2017). To investigate the mechanisms generated in this environment further, it is desirable to characterise the system over a wider range of tip amplitudes to understand all the conditions, which are generated as the tip amplitude of the HIU source (the PLE in this case) was varied. To do this, a set of experiments were performed looking for the conditions required to generate a 'clear' acoustic signature. Note that between these clear 'notes', a mixed response (where the audible emission is notably different) was observed. This corresponds to a less well-defined or mixed cluster behaviour. Figure 1 shows the frequency components obtained from the acoustic signature recorded as the PLE drive conditions were changed. Here the amplitude of the PLE tip oscillation (a Misonix S-3000 system that is a more powerful source than the Misonix XL2000 system) was altered and the acoustic emission from a bubble populated liquid oil analysed to determine the frequency components present. Figure 1 is arranged to show the lowest power inputs at the base and the highest at the top (see legend). Note in these experiments, the data was recorded in the steady state (e.g. the PLE was driven continuously while the data was captured) and that the experiments were recorded sequentially from low to high with respect to the energy input. Figure 1 shows that at the lowest power inputs employed (3 W, —) a single subharmonic peak was detected indicating an $f/2$ component generated at the tip. Imaging with a high-speed camera is inconclusive under these conditions. Bubble events are observed (not shown) but the origin of the emission may be either general cavitation bubble dynamics (Lauterborn, Kurz, 2010) or cluster behaviour. As the reported power of the HIU source was increased, the acoustic emission changed and two subharmonic emissions appeared (9 W, —). This was attributed to a cluster with an $f/3$ frequency. However, increasing the power input further yields a single subharmonic at ~ 12 W (Figure 1, —). This was accompanied by a change in shape of the cavitation plume observed by eye. Under these conditions the streamer that formed appeared to split into two (all other clusters produced a single streamer moving away from the PLE tip). This streamer is termed a 'bifurcated streamer' (BiS). Further characterisation of this unusual event was obtained using high-speed imaging of the system (see later discussion and Figure 3). The generation of the BiS event was accompanied by a district drop in the audible output of the cell (as determined by ear and shown in Figure 1 as a largely featureless region from 0-15 kHz except for a single peak at ~10 kHz). Increasing the power input further allows for clusters with different periodicity (with higher *N* values in the range 4-7) to be observed. Here, under these experimental conditions, a cluster with an *f*/7 frequency can be generated at the higher end of the power applied. Presumably, this upper limit was determined by the possible power output of the PLE employed in this study and the tip dimensions. This data also allows us to map the regions in power (and the PLE oscillation amplitude) where different behaviours can be generated. Figure 2 shows that as the drive stimuli was increased (as indicated by the power in watts reported by the amplifier), the order of the cluster climbs. Included in this figure is a measure of the actual tip amplitude (zero-to-peak) determined from independent high-speed camera experiments. These results suggest that the origin of the 'clear' audible note from the experimental system are these remarkably stable clusters with a consistent period of oscillation. The audible notes in turn are representative of the set of subharmonics, which are generated. This contrasts with the general 'hiss' associated with the so called 'white noise' generation often associated with cavitation(Young, 1999) itself and when mixed cluster behaviour is generated.

Characterization of the bifurcated streamer: Amongst the set of experimental investigations discussed above, an unusual BiS event was observed in the bubble populated media. This occurred at power inputs between an *f*/3 and *f*/4 cluster (see Figure 1 and 2). Further evidence for the mechanism driving this bifurcated behaviour can be gathered from high-speed imaging of the clusters that form under these conditions. Figure 3 shows a set of images obtained of a bifurcated streamer formed during sonication . Here the images were obtained at 150 kfps and a suitably fast shutter speed. The 14 images shown represent a single period of the clusters observed. In this case the imaging shows clear evidence for the origin of the BiS event, specifically two small clusters operating 180^0 out of phase (labelled C1 and C2 in Figure 3). In each case the cluster has a period of 93 ± 7 μs (14 ± 1 frames of the high-speed image shown in Figure 3). This represents 2 periods of the 22.5 kHz (44 μs)

PLE source employed. However, as there are two clusters, which oscillate out of phase (e.g. an 180^{o} phase shift with respect to one another), the acoustic emission will be composed of a pressure pulse every cycle of the acoustic drive. The frequency analysis reflects this behaviour with a weak emission centred on $f/2$, which presumably suggests a non-ideal nature of the pressure pulses produced or the conditions within the cell (non-uniform shielding, for example). Moreover, the bifurcated cluster/streamer represents a $f/2+(f/2)'$ case (where the ' indicates a 180^{o} phase shift of one cluster with respect to the other cluster) which appears between the $f/3$ and $f/4$ clusters. The two bubble streams that are produced in this case (see Figure 3) also show that the streams are strongly associated with the individual clusters. The high-speed imaging show that these streams change in intensity as each cluster produces shocks on collapse. These pressure shocks compress all the bubbles present in the local vicinity and cause rebounds, termed transient flashes (Birkin, Offin, Vian, Leighton, 2011) within both streamers. These dynamics help explain the unusual acoustic emission as both clusters contribute to the acoustics and presumably form a ‘dipole’ like weak emission (Kinsler, Frey, Coppens, Sanders, 1982). The exact conditions necessary for the BiS event are unclear at this time. It seems plausible that a combination of the physical properties of the oil (viscosity, gas content etc.) play a role. However, further exploratory experiments are necessary to fully elucidate this phenomenon, which are beyond the scope of the current work reported here.

Characterization of the bubble cluster: Previous imaging of the bubble clusters produced in these oil environments indicated that the collapse phase of the cluster involved an elaborate structure. This structure was assigned as consisting of an ‘arrowhead’, ‘neck’ and ‘ring’ section (Birkin, Foley, Truscott, Merritt, Martini, 2017). Further finer details on this process are now possible. Figure 4 shows a high-speed image sequence obtained at 300 kfps and a suitably fast shutter speed (1.726 µs). This high frame rate, accompanied with the camera resolution employed, allows for more details of the collapse phase to be obtained. Figure 4 image A0 shows the arrowhead, neck and ring structure annotated as (i), (ii) and (iii) respectively. In addition, an elongated bubble reported previously (Birkin, Foley, Truscott, Merritt, Martini, 2017) is highlighted with an arrow and bubbles B_1 and B_2 are marked and used to highlight the pressure pulses generated in the local environment close to the cluster. The sequence of frames A0-B3 shows that the entire structure (arrowhead, neck and ring) initially start to collapse together. However, B4 shows that a ring or disk of bubbles starts to reform on the surface of the PLE surface. This is labelled '(iii)' in frame C1. The full collapse of the arrowhead and neck is seen in frame C3 and a compression and rebound event seen through changes in bubbles B_1 and B_2 in frame C3-C4 (assigned TS_1). However, the ring remains, and this collapses slightly later in frame D3. This second collapse is also accompanied with a compression and rebound event for B_1 and B_2 highlighted in frames D3-4 (assigned as TS_2). The following frames E0-5 then show the cluster starting to reform. The second collapse (TS_2) and rebound events appear more significant in that most of the bubbles in view in D3 appear compressed (and many disappear from view at this resolution). This suggests that the pressure shock generated at this point is the highest in the sequence. This high-speed sequence suggests that the cluster collapse generates at least two shocks, which cause bubble compression and rebound in the local vicinity of the PLE tip. Further supporting evidence for this two-stage collapse process can be gathered by looking at the laser scattering data obtained under these conditions. Figure 5 shows examples of the scattering transient events caused by the cluster collapse under similar conditions. In this case, two transient light scattering events are often detected and accompanied by pressure pulses. Figure 5 demonstrates that the first collapse (which we presume would be associated with TS_1 on Figure 4) is significantly weaker than the second collapse (which we presume would be associated with TS_2 on Figure 4). This is highlighted in Figure 5 which shows that the first collapse (Figure 4 TS_1) was accompanied with a smaller transient change in the light scattering (Figure 5 orange arrows) through the oil and a weak pressure pulse detected by the hydrophone. Whereas the second collapse (marked as TS_2 on figure 4) is accompanied by a larger transient change in the light scattering through the oil (Figure 5 blue arrows) and a larger pressure pulse. Note the pressure pulses detected by the hydrophone are detected ~ 13 µs later which is in reasonable agreement with the speed of sound in oil (Kaye, Laby, 1959) (1440 m s^{-1}) and the distance between the PLE and the hydrophone (15 ± 5 mm). The timing between the two collapses is estimated from the laser scattering data as 10-14 µs in good agreement with the high-speed camera data shown in Figure 4. The magnitude of the light scattering events and the pressure pulses detected by the hydrophone suggest that the second collapse is more intense in nature. This is in agreement with the high-speed sequence shown in Figure 4.

Conclusions

The generation of clusters at an PLE tip in the oil/lipid system shows some remarkable characteristics. The acoustic emission, high-speed imaging and scattering data show that the PLE tip amplitude plays a key role in the dynamics of the cavitation cloud. The cavitation cloud in the oil systems forms a set of well-defined clusters which collapse under the conditions employed at a variety of different frequencies (here ranging from $f/2$-$f/7$) relating to the amplitude of the PLE tip zero-to-peak displacement. A 'bifurcated streamer' can also be generated within this system. This has been shown to originate from two clusters oscillating at a frequency of $f/2$ with an 180° phase shift between them. Finally, the collapse phase of the clusters generated has been shown to occur in a two-stage process. This process generates two transient flashes(Birkin, Offin, Vian, Leighton, 2011) (bubble compression and rebound) and are accompanied by pressure pulses within the fluid.

Acknowledgements

This project was supported by Agriculture and Food Research Initiative (AFRI) Grant No. 2017-67017-26476 from the USDA National Institute of Food and Agriculture, Improving Food Quality–A1361. This project was approved by the Utah Agricultural Experiment Station as Project Number 9045. PRB would like to thank Photron and, in particular, Tim Nichols for their assistance with some of the high-speed imaging.

References

Birkin, P. R., Foley, T. M., Truscott, T. T, et al (2017) Cavitation clusters in lipid systems – surface effects, local heating, outgassing and streamer formation. Physical Chemistry Chemical Physics **19**:6785–6791

Birkin, P R, Foley, T M, Truscott, T T, et al (2017) Cavitation clusters in lipid systems-surface effects, local heating and streamer formation †. Phys Chem Chem Phys **19**:6785. https://doi.org/10.1039/c6cp08149e

Birkin, Peter R, Leighton, Timothy G, Power, John F, et al (2003) Experimental and Theoretical Characterization of Sonochemical Cells . Part 1 . Cylindrical Reactors and Their Use to Calculate the Speed of Sound in Aqueous Solutions. Journal of Physical Chemistry A **107**:306–320

Birkin, P R, Offin, D G, Joseph, P F, Leighton, T G (2005) Cavitation, shock waves and the invasive nature of sonoelectrochemistry. Journal of Physical Chemistry B **109**:16997–17005. https://doi.org/10.1021/jp051619w

Birkin, Peter R, Offin, Douglas G, Vian, Christopher J B, Leighton, Timothy G (2011) Multiple observations of cavitation cluster dynamics close to an ultrasonic horn tip. Journal of the Acoustical Society of America **130**:3379–3388. https://doi.org/10.1121/1.3650536

Chen, F, Zhang, H, Sun, X, et al (2013) Effects of ultrasonic parameters on the crystallization behavior of palm oil. Journal of the American Oil Chemists' Society **90**:941–949

Chow, R., Blindt, R., Chivers, R., Povey, M. (2005) A study on the primary and secondary nucleation of ice by power ultrasound. Ultrasonics **43**:227–230

Chow, R., Blindt, R., Kamp, A., et al (2004) The microscopic visualisation of the sonocrystallisation of ice using a novel ultrasonic cold stage. Ultrasonics Sonochemistry **11**:245–250

Flint, E B, Suslick, K S (1991) The Temperature of Cavitation. Science **253**:1397–1399

Hansson, I, Kedrinskii, V, Morch, K A (1982) On the dynamics of cavity clusters. Journal of Applied Physics D: Applied Physics **15**:1725–1734

Hansson, I, Morch, K A (1980) The dynamics of cavity clusters in ultrasonic (vibratory) cavitation erosion. Journal of Applied Physics **51**:4651–4658

Higaki, K, Ueno, S, Sato, K (2001) Effects of ultrasonic irradiation on crystallization behavior of tripalmitoylglycerol and cocoa butter. Journal of the American Oil Chemists' Society **78**:513–518

Kaye, G W C, Laby, T H (1959) Tables of Physical and Chemical Constants and some Mathematical Functions, 12th ed. Longmans, Green and Co, London

Kinsler, L E, Frey, A R, Coppens, A B, Sanders, J V (1982) Fundamentals of Acoustics. John Wiley & Sons, New York

Lauterborn, Werner, Kurz, Thomas (2010) Physics of bubble oscillations. Reports on Progress in Physics **73**:106501. https://doi.org/10.1088/0034-4885/73/10/106501

Martini, Silvana, Tejeda-Pichardo, R., Ye, Y., et al (2012) Bubble and Crystal Formation in Lipid Systems During High-Intensity Insonation. Journal of the American Oil Chemists' Society **89**:1921–1928. https://doi.org/10.1007/s11746-012-2085-z

Offin, D G (2006) Acoustoelectrochemical characterisation of cavitation and its use in the study of surface processes. University of Southampton

Patrick, M, Blindt, R, Janssen, J (2004) The effect of ultrasonic intensity on the crystal structure of palm oil. Ultrsonics Sonochemistry **11**:251–255

Price, Gareth J (1992) Introduction to Sonochemistry. The Royal Society of Chemistry, Cambridge

Price, Gareth J., Ashokkumar, Muthupandian, Grieser, Franz (2003) Sonoluminescence Emission from Aqueous Solutions of Organic Monomers. The Journal of Physical Chemistry B **107**:14124–14129. https://doi.org/10.1021/jp034375t

Price, G J, Lenz, E J (1993) The use of dosimeters to measure radical production in aqueous sonochemical systems. Ultrasonics **31**:451–456

Suslick, K S, Hammerton, D A, Cline, R E (1986) The Sonochemical Hotspot. Journal of the American Chemical Society **108**:5641–5642

Suzuki, A, Hartel, R W, Martini, S (2010) Altering functional properties of fats using power ultrasound. Journal of food science **75**:E208–E214

Ueno, S, Ristic, R.I, Higaki, K, Sato, K (2003) In situ studies of ultrasound-stimulated fat crystallization using synchrotron radiation. Journal of Physical Chemistry B **107**:4927–4935

Vyas, B., Preece, C. M. (1976) Stress produced in a solid by cavitation. Journal of Applied Physics **47**:5133–5138. https://doi.org/10.1063/1.322584

Weissler, A, Cooper, H W, Snyder, S (1950) Chemical effect of ultrasonic waves: oxidation of potassium iodide solution by carbon tetrachloride. Journal of the American Chemical Society **72**:1769–1775

Whillock, G O H, Harvey, B F (1997) Ultrasonically enhanced Corrosion of 304L Stainless Steel II: The effect of frequency, acoustic power and horn to specimen distance. Ultrasonics Sonochemistry **4**:33–38

Ye, Y, Martini, S (2015) Application of high intensity ultrasound to palm oil in a continuous system. Journal of agricultural and food chemistry **63**:319–327

Ye, Y, Wagh, A, Martini, S (2011) Using high intensity ultrasound as a tool to change the functional properties of interesterified soybean oil. Journal of agricultural and food chemistry **59**:10712–10722

Young, F R (1999) Cavitation. Imperial College Press, London

Zhong, H, Allen, K, Martini, S (2014) Effect of lipid physical characteristics on the quality of baked products. Food Research International **55**:239–246

Captions

Fig. 1 Plots showing the frequency characteristics of the acoustic emission from an SBO system as a function of reported wattage employed. The symbols indicated the subharmonics detected at points during the experiment. Here (♦) represents the subharmonic emissions associated with stable clusters, while (♦) represents the possible position of the bifurcated streamer. Experiments performed in soybean oil, SBO (23-40 ^{o}C). Hydrophone positioned ~ 15 mm from the PLE tip. The grey section shows the fundamental (~19.9 kHz). The stimuli (determined by the instrumentation) were 3, 9, 12, 21, 36, 54 and 84 W for ▬, ▬, ▬, ▬, ▬, ▬ and ▬ respectively (moving from the base of the figure to the top).

Fig. 2 Plot showing the reported power (RP, ●) and the measured zero-to-tip amplitude (♦). The error bars are calculated from the uncertainty estimated for the image analysis. The experiments relate to SBO. The number in parenthesis indicated the periodicities (*N*) observed (through acoustic analysis). 'B' indicated where the bifurcated streamer was observed.

Fig. 3 Images showing the growth and collapse of two clusters responsible for the bifurcated streamer (BiS) in sunflower oil. The images were recorded at 150 kfps and a 5 μs shutter speed. The red highlight squares show the complete period of the cluster on the right (C2) while the yellow highlight shows the time where the left cluster has collapsed (C1). The sunflower oil was maintained at ambient conditions (~24 ^{o}C). The scale bar represents 1 mm. The frames should be viewed from top left in a raster like fashion. The PLE tip (3.2 mm diameter) was driven at 9 W_{rms}. S1,2 shows the motion of the two streams generated and the arrows their associated motion in the cell.

Fig. 4 Images showing the collapse of an *f*/5 cluster. The images were recorded at 300 kfps and a 1.726 µs shutter speed. The frames should be viewed from top left in a raster like fashion (e.g. A0 to A4 then B0 to B4 and so on). The PLE tip (3.2 mm diameter) was driven at 26 W_{rms}. Frame A0 shows the arrowhead, neck and ring ((i), (ii) and (iii)) respectively as well as an elongated bubble (orange arrow) and two highlighted bubbles (B_1 and B_2) are used for reference and are discussed in the main text. The highlight squares (TS_1 and TS_2) represent the two transient collapse processes. The sunflower oil was maintained at ambient conditions (~24 °C). The scale bar (D0) represents 1 mm.

Fig. 5 Plot showing the laser scattering signal from the photodiode (PD) (**—**) and pressure data (**—**) as a function of time recorded for an experiment in bubble at 32 W_{rms} setting on the PLE. The orange arrows (↓) mark the positions of the TS_1 collapse and the blue arrow (↓) collapse TS_2. The laser path was ~ 2.5 mm below the PLE.

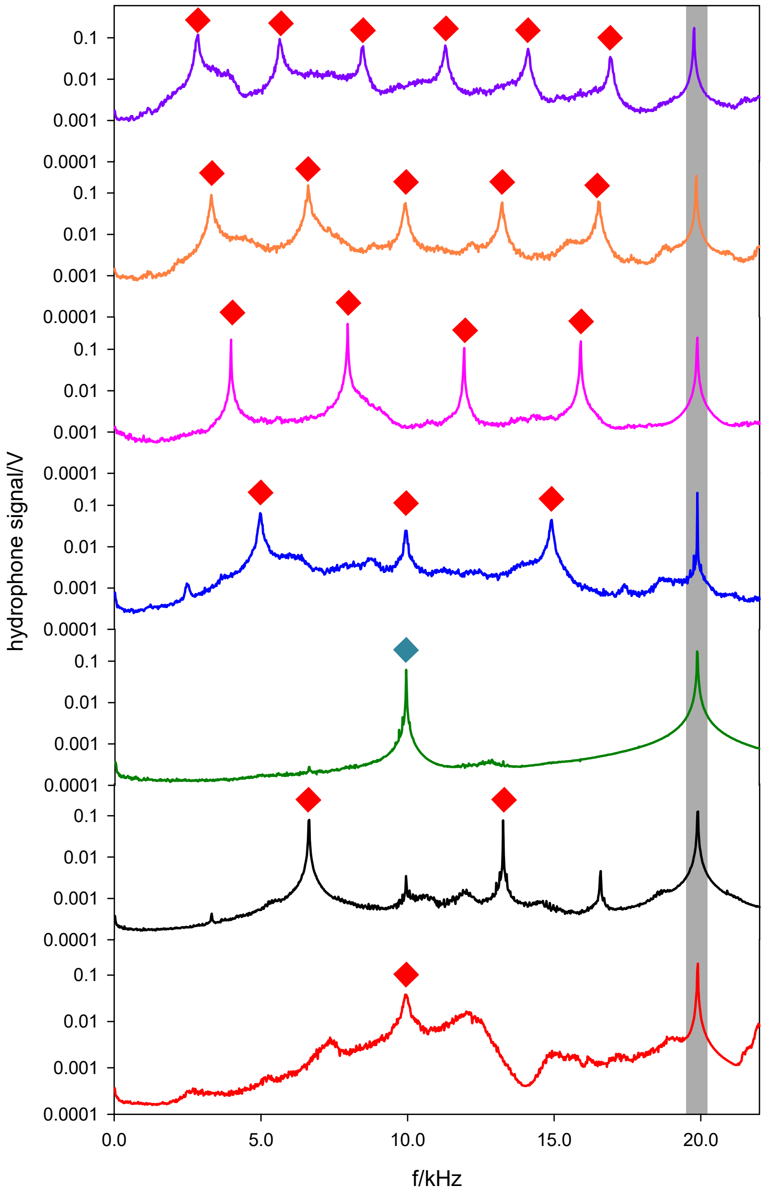

Fig. 1

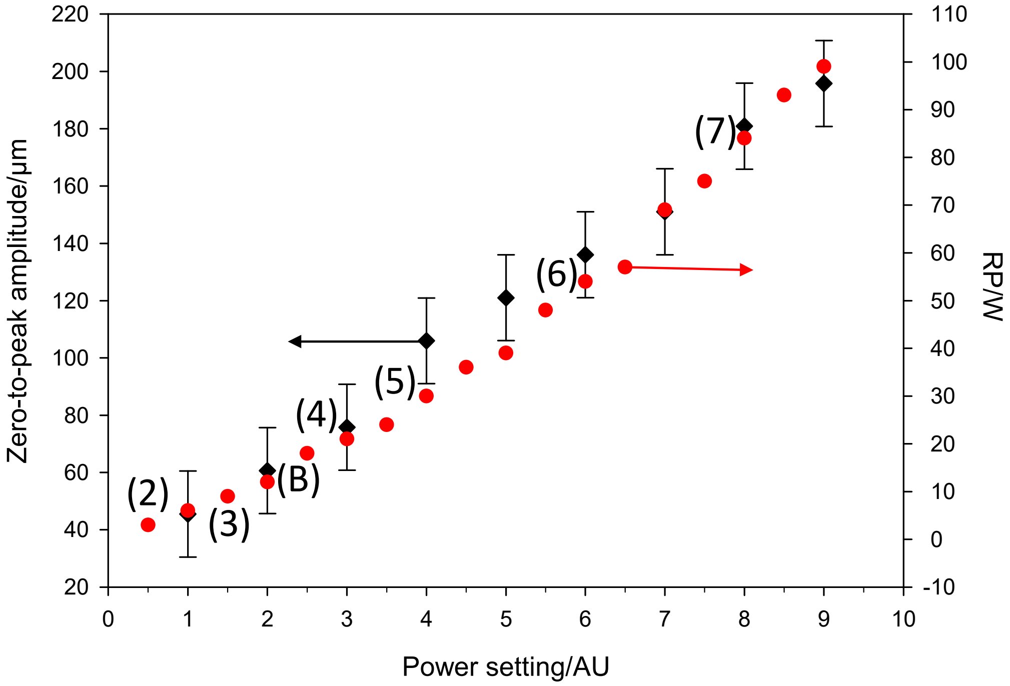

Zero-to-peak amplitude/μm
RP/W
Power setting/AU
220
200
180
160
140
120
100
80
60
40
20
110
100
90
80
70
60
50
40
30
20
10
0
-10
0
1
2
3
4
5
6
7
8
9
10
(2)
(3)
(B)
(4)
(5)
(6)
(7)

Fig. 2

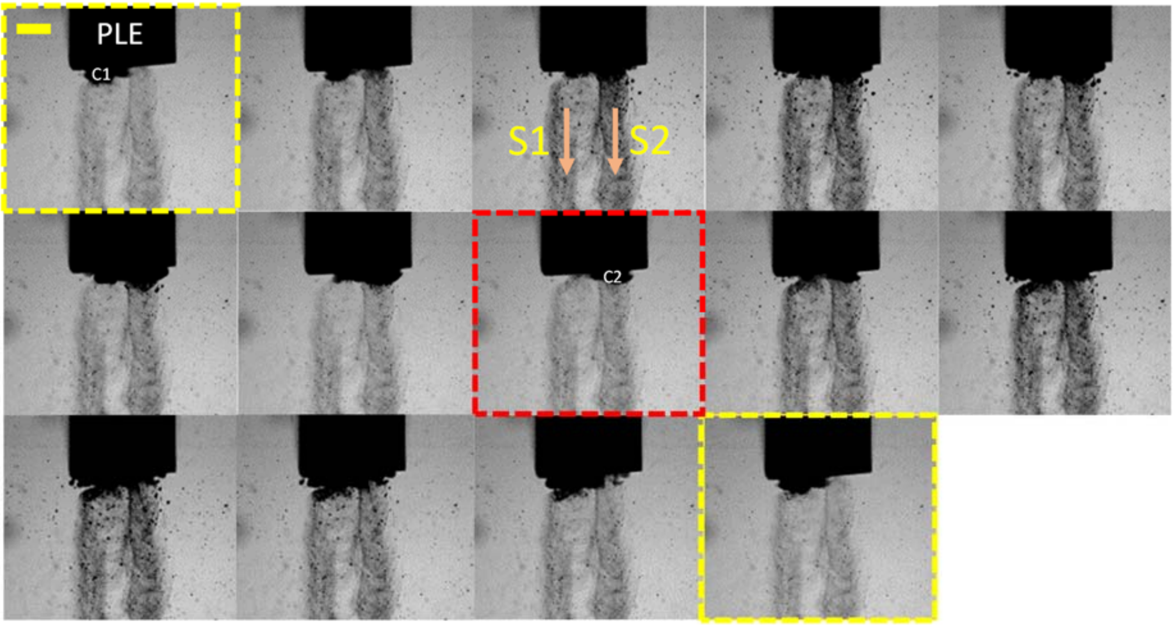

Fig. 3

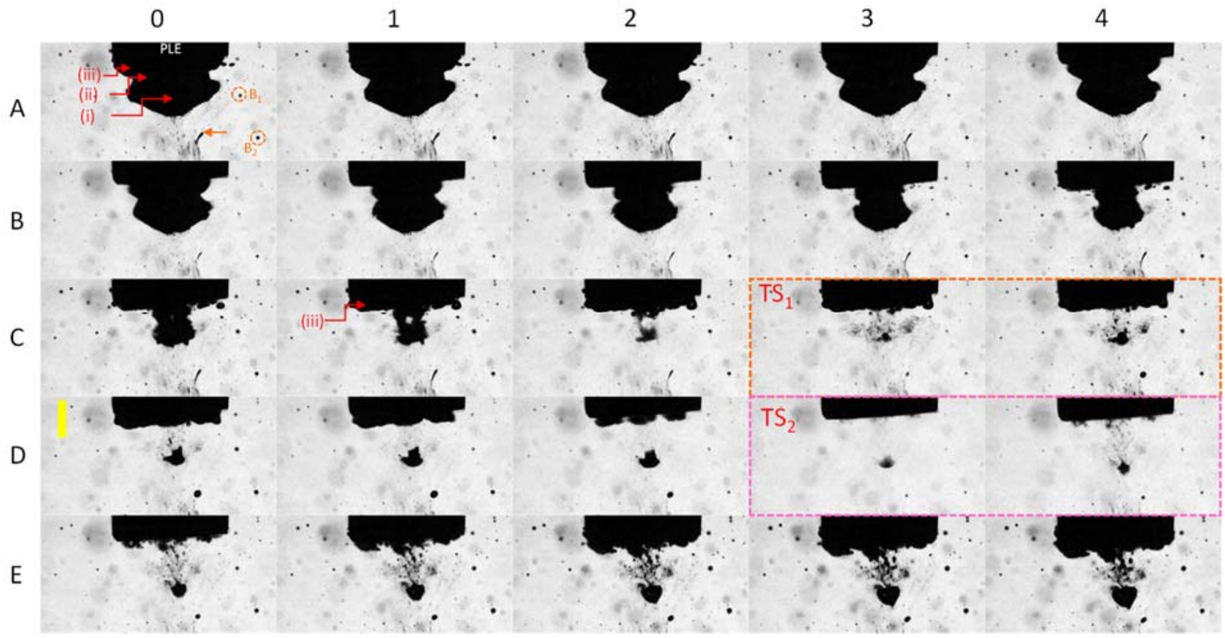

Fig. 4

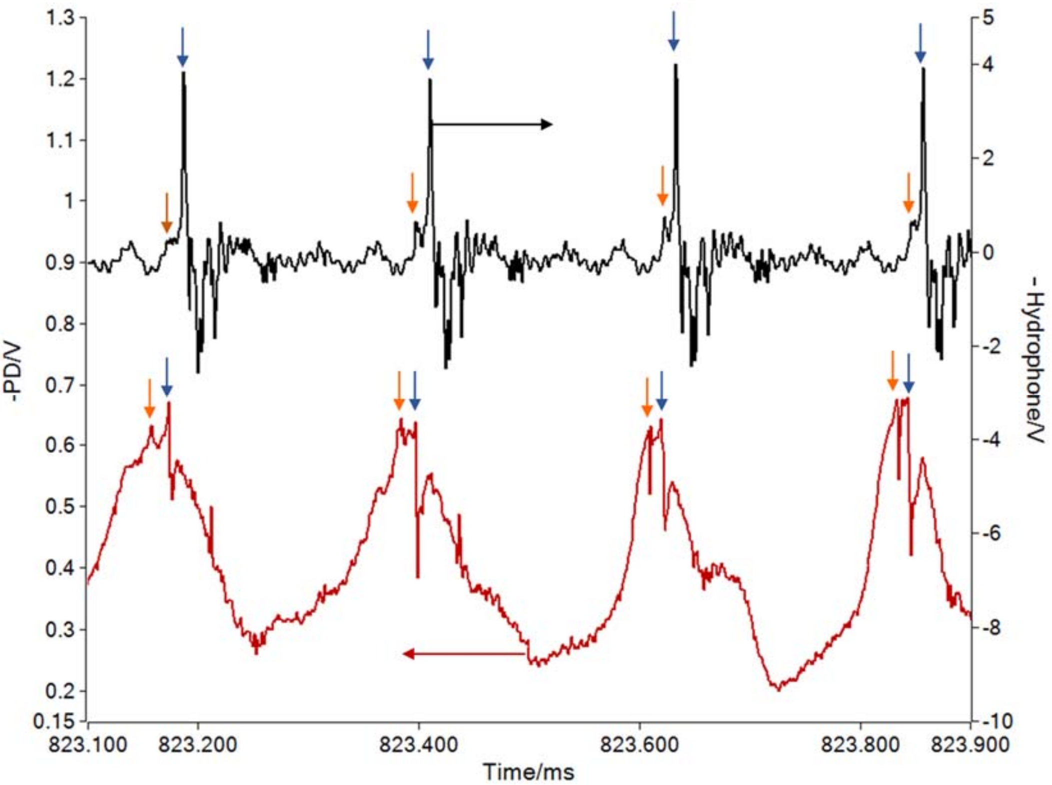

1.3
1.2
1.1
1
0.9
0.8
0.7
0.6
0.5
0.4
0.3
0.2
0.15
-PD/V
5
4
2
0
-2
-4
-6
-8
-10
- Hydrophone/V
823.100
823.200
823.400
823.600
823.800
823.900
Time/ms

Fig. 5